DSmT based Ultrasonic Detection Model for Estimating Indoor Environment Contour

Shuai Yuan, *Member, IEEE,* Pengcheng Guo, Xiaoying Han, Fangjun Luan, Feng Zhang, Tianbo Liu, and Hongmin Mao

***Abstract*—As for uncertainties of ranging and direction angle in the ultrasonic sensor measurement, an ultrasonic distance measurement model is first of all proposed for representing these uncertainties through analyzing working principle of the ultrasonic sensor, which can be adopted to detect the contour of wall plan and cylinder. Moreover, the Dezert-Smarandache Theory (DSmT) method is employed to fuse the uncertainty data measured by using the ultrasonic sensor. Next, Extended Hough Transform (EHT) and Least Square Method (LSM) are combined to identify the environmental contour. Then the measurement uncertainty of the ultrasonic sensor is analyzed for setting the threshold Th used for distinguishing line and cylinder, and detection range of the cylinder radius is estimated. Finally, we build an indoor environment and design the ultrasonic sensor hardware system to detect the indoor environment for experimental verification. The indoor environment contour obtained in the experimental results is consistent with the real environment, which illustrate the feasibility and effectiveness of the proposed method. The proposed method has certain reference value for research of simultaneous localization and mapping (SLAM) of the mobile robot.**

***Index Terms*—Ultrasonic sensor, DSmT fusion, Hough transform, Least squares method, SLAM.**

I. Introduction

MOBILE robots, like humans, rely on maps to perceive the external environment for estimating their position. Robot navigation is a key technology for mobile robot research.The technology includes localization, mapping and path planning. The mapping is the basis of localization and path planning. The ultrasonic sensor perceives information about the environment surrounding the robot by transmitting ultrasonic energy pulses and receiving reflected echoes. The sonic velocity and transit time are used to estimate the position of the reflector.

The sensing technologies currently adapted mainly include laser sensing technology, visual sensing technology, ultrasonic sensing technology and infrared sensing technology. Among them, the cost of laser is relatively high, the detection distance is far away, and it is not affected by ambient light. It is costly for indoor environment contour detection and cannot fully exert its advantages, and cannot make the best use of it. In addition, the laser classification of the object is limited, and when there is a glass wall in the room, there is no reflection information and there are blind spots. Compared with laser sensors and vision sensors, ultrasonic sensors are cost-effective and easy to control[1-3]. They have become a common detection method for mobile robots to detect their surroundings and acquire features of unknown environment contour [4-6].

It is usually considered that there are three different levels in ranging ultrasonic systems: low level processing (at the signal level) such as signal coding, matched filter, etc; medium level processing (at the sensor level) such as transducer arrangement, firing strategies, sensor models, etc; and high level processing (at the application level) such as object recognition, reflector classification, etc.

In the above three levels of research, due to the uncertainty of ultrasonic sensor measurement[7], there are two shortcomings: (1) There is a certain error in the distance measurement value; (2) The sonar sensor has typically a certain range of sight, and large beam angle has a considerable uncertainty in measurement orientation [8, 9].

In low level processing (at the signal level), [10] designed a high-resolution adaptive spiking sonar, which is capable to obtain bearing information from the spikes generated in the 'auditory nerves' of both ears by mimicking their neural circuitry, but the algorithm is complex; The method proposed in [11] reconstructs the environment by comparing the binaural spectral template of existing echoes with one of the returned echoes from different angles. [12] estimates location and orientation of the target by extracting a detected arc of ultrasonic scan. Both of the abovementioned methods can improve detection accuracy of the object position through multiple measurements, but these detection methods are lack of flexibility and adaptability. [13] developed a data association filter (DAF) which built a probability grid map for representing environment contour information, improving reliability of data and reducing error caused by measurement errors. However, grid maps constructed by ultrasonic sensors cannot implement a realistic representation of a given environment [14].

In medium level processing (at the sensor level), errors are further reduced. In [15], every two transducers constitutes a "vector sensor" and enough precision and reliability of

Manuscript received Feb.26, 2019. This research work is partially supported by the National Natural Science Foundation of China (Project Codes:61703288), and Liaoning Colleges and Universities basic Scientific Research Project (LJZ2017020) Liaoning Province Natural Science Foundation (20180520037).(*Corresponding author: Fangjun Luan.*)

S. Yuan is with the school of Information & Control Engineering, Shenyang Jianzhu University, Shenyang, Liaoning Province 110168, China, and also is with the State Key Laboratory of Robotics, Shenyang Institute of Automation, Chinese Academy of Sciences, Shenyang, Liaoning Province 110016, China. (Emai:reidyuan@163.com).

P.C. Guo, X.Y.Han, F.J. Luan, F. Zhang, T.B. Liu and H.M. Mao are with the school of Information & Control Engineering, Shenyang Jianzhu University, Shenyang, Liaoning Province 110168, China.

Hongmin Mao are with CCTEG Shenyang Research institute, Shenyang, Liaoning Province 110168, China.

time-of-flight (TOF) is improved, and the map is finally drawn. When measuring in a two-dimensional system, the ultrasonic sensor captures multiple detection distances for multiple sampling times over a period. These distance detection values are uniformly distributed random points within annular-sector domain, then a brightness scan (B-scan) [16] is displayed as the distribution density of these random points. The method focuses on using statistical data to extract the shape and contour of the measured object; however, it does not reduce the orientation uncertainty of measurement. [17, 18] provided a grid map building method based on fuzzy logic operations. And [19] developed a single echo ranging model based on information fusion. Furtherly, our preliminary work [20] adapted the DSmT data fusion method to establish an ultrasonic sensor detection model, using probabilistic methods to estimate the position of obstacles, reducing the distance error and direction uncertainty during ultrasonic measurement, but it lacks effective environmental contour detection and environmental description methods. In a three-dimensional system, in order to effectively reduce the noise disturbance and direction uncertainty in the ultrasonic measurement procedure, [21] proposed to integrate multiple ultrasonic sensors, using the microphone array and hardware integration technology to achieve ultrasonic 3D measurement and to accurately determine 3-D target locations over a wide field of view (FOV) using simple delay and post-processing for allowing real-time performance.

In the application-level study of ultrasonic ranging, [22] adapted principal component analysis (PCA) and time-of-flight (TOF) as parameters to identify reflector type by using different designed macro sequence for every transducer encoding their emissions and acquiring three-dimensional position information. [23] presented a solution to combine a novel 3D sonar sensor with BatSLAM mapping module, which simply environment descriptors. By combining odometric information derived from the 2D energy field with the one of the 3D energy field, the position of the robot can be correctly estimated, and the trajectory of the robot is reconstructed, and the function of obstacle avoidance navigation is realized. Based on these work, [24] simplified the hardware system, used low-cost digital MEMS microphones to achieve ultrasound imaging, and verified its practicality of extended microphones array.

In the abovementioned research work, the three basic contours of the experimental environment are plane, corner and cylinder, and the former two types has been effectively extracted and identified.During detection of the corner, which can lead to a double bounce of the ultrasonic signals, measurements are completely confused due to the secondary reflection. Considering that the corner is composed of two walls, that problem can be resolved by reconstructing the corner according to these two walls information. In this paper, the basic contour is furtherly simplified into walls and cylinders, and the two are detected, identified and classified. At the sensor level, firstly, sensor detection model is established and the reliability function is designed to calculate the measured data reliability and extract feature points. Secondly at the application level, EHT and LSM are combined to recognize the feature points and reconstruct contour so as to reduce the uncertainty of ultrasonic sensors; then the uncertainty of the measurement data of the ultrasonic sensor is analyzed by statistical experiments, and the parameter setting and the radius of the cylinder detection radius are estimated. Finally, the proposed work are verified through building an indoor environment and designing a detection control system. The experimental results illustrate the effectiveness of the proposed method.

The structure of this paper is arranged as follows. Ultrasonic sensor detection model based on uncertainty representation is given in Section II. In Section III, contour model based reliability region detection is proposed. EHT and LSM are combined to estimate the environment contour in Section IV. Ultrasonic sensor uncertainty analysis, parameter setting, and discussion on measurement range of cylinder radii is represented in Section V. Experiment is performed and analyzed for illustrating the proposed method efficiency in Section VI and finally the conclusion is obtained in section VII.

II. ULTRASONIC SENSOR DETECTION MODEL BASED ON UNCERTAINTY REPRESENTATION

A. Ultrasonic detection model based on annular-sector region

The mathematical model is established according to physical characteristics of the ultrasonic sensor. Because the measurement distance of the ultrasonic sensor has error and orientation of measurement is uncertain, this paper proposes annular-sector uncertainty region instead of possible positions of detected objects, as shown in Fig.1. Fig.1 is a single ultrasonic detection model. R is the return distance data of the ultrasonic detection. The error range is represented by the shaded area of the sector, and ω is the angle range of the ultrasonic detection orientation, i.e. the beam angle. The detection direction of the measured data is within this range. Generally, ω is related to the characteristics of the ultrasonic sensor. According to the physical properties of the sonar, ω is set to 22.5°. ε that is the measurement error of distance R is 2 mm. The annular-sector area in Fig.1 represents distance inaccuracy and direction uncertainty of the ultrasonic sensor.

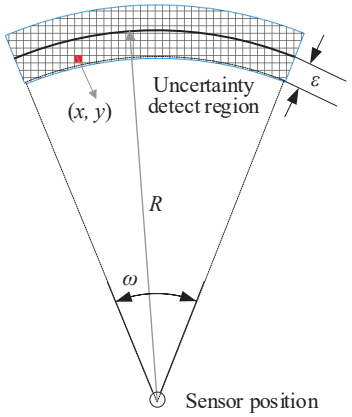

Fig.1 Ultrasonic detection model by using uncertainty representation.

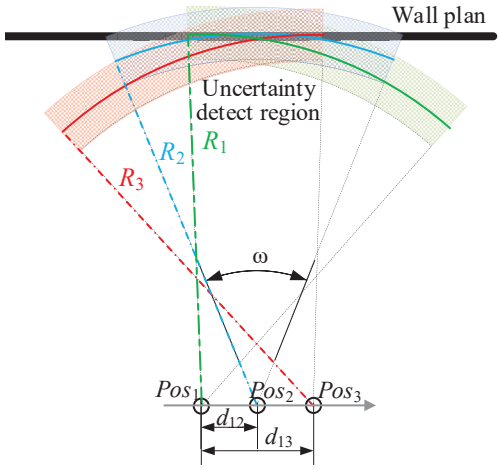

(a) Wall plan contour.

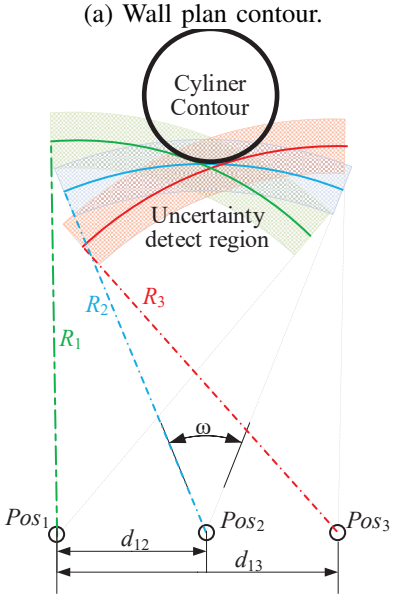

(b) Cylinder contour.

Fig.2. Ultrasonic sensor measurement result at three positions

B. Wall and Cylinder Contour Detection based on Multiple Measurements

In order to improve accuracy of measurement, this paper adopts DSmT method[25] for data fusion of multiple measurements, and updates the map to improve accuracy of measurement data. Fig. 2 shows three measurements of the ultrasonic sensor detecting different environmental contours at three adjacent locations P_{os1}, P_{os2}, P_{os3}, and Fig. 2.(a) shows the wall plan contour, and Fig.2.(b) shows the cylinder contour. The overlapping area of three measurement results in figure is the area where the sector region contacts wall plan or cylinder. Then DSmT method is used to fuse the results of multiple measurements to improve accuracy of the detected data. In this paper, we first distinguish the two environmental contours of straight line and circular arc. Two types of environmental contours are selected by two detection model and identification methods. Below we propose a method to distinguish two types of environmental contours. We define a parameter R_{2d}, which is a referential arc radius between R_1 and R_3. The definition is expressed as follows:

$$R_{2d} = R_1 + (R_3 - R_1 \times d_{12}/d_{13}) \tag{1}$$

Comparing the parameters R_{2d} with R_2, if the difference is very small, there is a common tangent line on the measured arcs at three positions, that is, the detected contour is a wall plan; if the difference is too large, there is no common tangent line on the measured arcs at three positions, and there may be a externally common tangent circle, and it means that the detected contour is a cylinder. We set a threshold value Th to judge different types of environmental contours. The judgment conditions are as follows:

$$\text{ContourType} = \begin{cases} \text{Plan}, & \text{if } \mid R_{2d} - R_2 \mid < Th \\ \text{Cylinder}, & \text{if } \mid R_{2d} - R_2 \mid \geq Th \end{cases} \tag{2}$$

By rotating and multiple measurements, a single sonar sensor measurement can be equivalent to the simultaneous measurement of multiple sonar sensors, whose data is used to estimate the environmental contour. Therefore, this method can also be used to detection of multiple sensors and environment reconstruction.

III. CONTOUR MODEL BASED ON RELIABILITY REGION DETECTION

The multiple measurements are performed for the same detected cylinder, then abovementioned sonar detection model is used to represent contour and then data fusion method is adopted to processing these data for promoting measurement accuracy, which runs with high efficiency in real-time and has many practical application.

A. Basic principles of DSmT

Dempster Shafer Theory (DST) has obtained the extensive attention of researchers of information fusion; the main reason is that it is a brilliant mathematical model in dealing with uncertain information. It takes Bayes theorem as its special case and carries out abstract mathematical representation of information fusion. Due to shortcomings and limitations of that method, DSmT method [20] has been proposed for further developing the DST. DSmT can process information obtained from k independent sources and fuse data. In procedure of fusion, the conflict factor, $k_{1,2\ldots s}$, is generated. Dempster improves DST through reassigning the total conflict quality to a propositional space using a simple normalization process. Due to counter-intuitive features of this DST rule in high conflicts, it has caused great controversy. However DSmT solves the problem of conflict allocation well, and there are many multiple distribution rules. In this paper, a PCR6 assignment method is used. The representation of this method is as following:

$$\forall(X \neq \emptyset) \in D^{\Theta}$$

$$m_{PCR6}(X) = \sum_{\substack{X_1, X_2, \cdots, X_s \\ X_1 \cap X_2 \cap, \cdots, X_s = X}} \prod_{i=1}^{s} m_1(X_i) + C(X)\frac{c_{12,\cdots,s}(X)}{e_{1,2,\cdots,s}} \bullet k_{1,2,\cdots,s} \quad (3)$$

Where $C(X)$ is

$$C(X) = \begin{cases} 1 & \text{if } X \text{ is related to the conflict item} \\ 0 & \text{else} \end{cases} \quad (4)$$

$C_{1,2,\cdots,s}$ is the sum of non-zero X, $k_{1,2\ldots s}$ is the collision factor, $m_i(\cdot)$ is the generalized reliability function, and $e_{1,2\ldots s}$ is the sum of the non-zero focal elements generating the amount of conflict.

B. Ultrasonic Data Fusion By Using Credibility

DSmT is adopted to represent the reliability of each grid (pixel) in the annular-sector region. θ_1 and θ_2 represent two situations of occupancy grid. θ_1 denotes the occupied grid and θ_2 denotes the unoccupied one. According to DSmT, we can get a hyper-power set $D^{\Theta} = \{\Phi, \theta_1, \theta_2, \theta_1 \cap \theta_2, \theta_1 \cup \theta_2\}$, where $\theta_1 \cap \theta_2$ means that it is both occupied and unoccupied as a conflict factor, and where $\theta_1 \cup \theta_2$ that it cannot be determined whether it is occupied. We can formulate the following reliability assignment functions (6), (7) and (8) based on the physical properties of ultrasonic sensor and the characteristics of actual measurement data.

$$\lambda = \begin{cases} 1 - (\frac{2\theta}{\omega}), & 0 \leq \theta \leq \frac{\omega}{2} \\ 0 & \text{others} \end{cases} \quad (5)$$

$$m(\theta_1) = \begin{cases} \lambda - \lambda \cdot \frac{|d-R|}{\epsilon}, & R - \epsilon \leq d \leq R + \epsilon \\ 0 & \text{others} \end{cases} \quad (6)$$

$$m(\theta_2) = \begin{cases} \lambda \cdot \frac{|d-R|}{\epsilon}, & R - \epsilon \leq d \leq R + \epsilon \\ 1 & \text{others} \end{cases} \quad (7)$$

$$m(\theta_1 \cup \theta_2) = \begin{cases} 1 - \lambda, & R - \epsilon \leq d \leq R + \epsilon \\ 0 & \text{others} \end{cases} \quad (8)$$

Since $\theta_1 \cap \theta_2$ is only generated during calculation, there is no need to adopt an assignment function [14]. In the above-mentioned formula, λ is the proportional coefficient of the reliability function, and depending on the angle θ. R is the distance from the sonar position to the obstacle; d is the distance from the sonar sensor position to the grid (x, y) (point (x, y) are the pixel coordinate of the sonar scanning region); θ is the angle between d and the central axis. ω is the beam angle of ultrasonic sensor set to 22.5°; ϵ is the error range of the sonar detect data, and it is set to 2 mm according to the physical properties of the sonar sensor. When the angle theta are the same, and λ is a fixed value, we have $m(\theta_1) = m(\theta_2) = \lambda/2$ and the conflict factor $m(\theta_1 \cap \theta_2)$ is the maximum, which satisfies the condition proposed by [19]. As can be seen from Fig.3, the closer to $R = 3.0$ m the detect distance is, the larger $m(\theta_1)$ is, while the $m(\theta_2)$ is opposite. Furthermore, the $m(\theta_1 \cup \theta_2)$ is only related to the angle θ, which would be more able to reflect the physical properties of uncertain direction. It is not enough to capture available information for realizing accurate environment contour by using single ultrasonic measurement, due to its uncertainty and inaccuracy. Here a remedy is to use multiple of ultrasonic measurements to fuse measurement data to reduce its uncertainty and increase the reliability of measurement data.

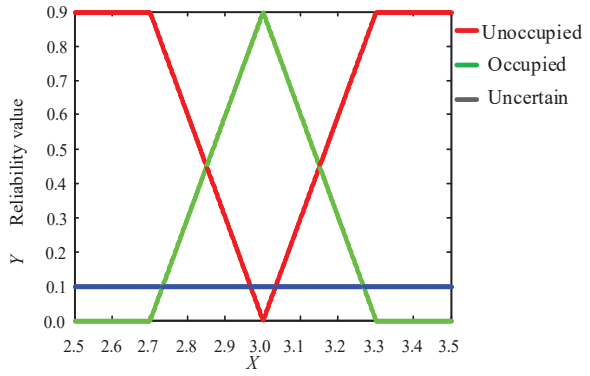

(a) The relationship between the grid reliability and the distance ρ when $\theta = 5°$.

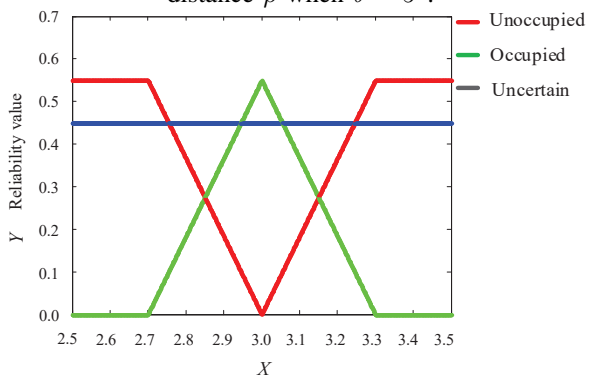

(b) The relationship between the grid reliability and the distance ρ when $\theta = 15°$.

Fig.3. The relationship between the grid reliability and the distance ρ when θ is set to difference value

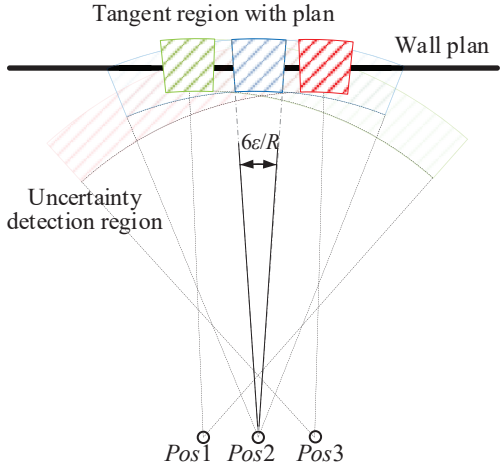

Fig.4. Contact areas of wall plan and annular-sector.

This article has been accepted for publication in a future issue of this journal, but has not been fully edited. Content may change prior to final publication. Citation information: DOI 10.1109/TIM.2019.2943715, IEEE Transactions on Instrumentation and Measurement

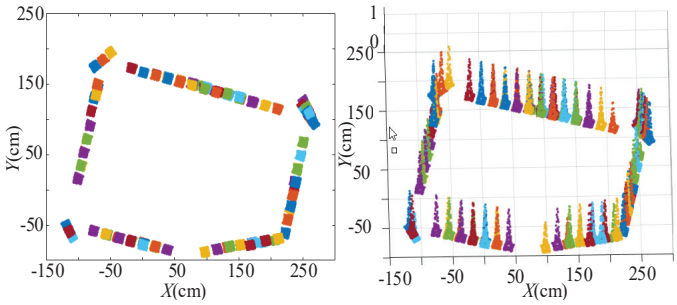

(a) Measurement reliability. (b) Pixels reliability of each area
Fig.5 Calculation of contact point reliability of wall plan.

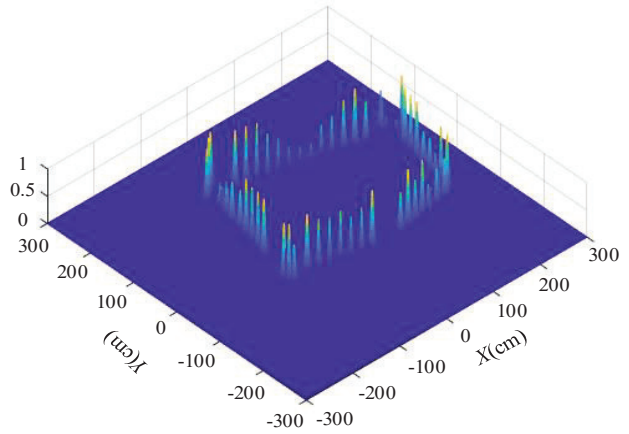

Fig.6 Detection result of wall plan reliability areas based on DSmT.

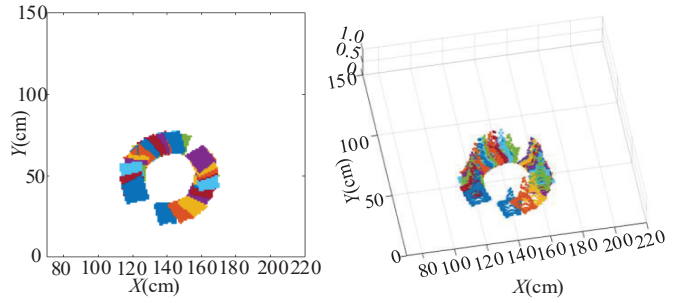

(a) Measurement reliability. (b) Pixels reliability of each area

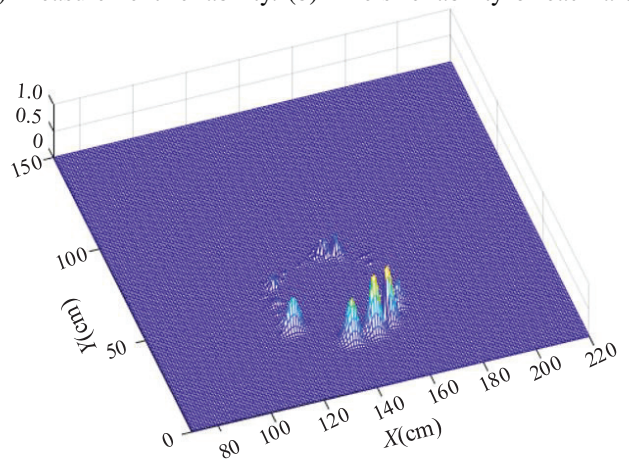

(c) The detection result of cylinder reliability areas
Fig.7 Calculation of cylindrical reliability using DSmT.

C. Reliability Representation based on Contact Point

The uncertainty area represented by annular-sector domain is large enough to make it difficult for accurate reconstructing the environmental contour. Therefore, on the foundation of a large number of measurements, we can consider the tangent region as detection region containing the common tangent line or common tangent arc, which is extracted as annular-sector region. Multiple sets of ultrasonic measurements are used to reduce the range of uncertain area [25]. We first represent the reliability area for the environment contour of wall plan as the linear type. As shown in Fig.4, there are some annular-sector region, which are tangent to the wall plan and whose central angle is $6\epsilon/R$. Those area include all of possible detected points of the wall plan and those points are the detected positions where ultrasonic waves are reflected when touching the wall plan. In reconstruction of the environmental contour, the detected points can be used to estimate the wall plan. Since multiple measurements can be used to reconstruct the environment contour, we can get multiple sector reliability regions, as shown in Fig.5.

Fig.5 (a) shows the reliability area for multiple measurements that overlap with each other. The value of reliability of pixels in each area is between 0 and 1, as shown in Fig.5 (b). Then DSmT method is adopted to fuse the data to furtherly obtain the reliability area. As shown in Fig.6, the higher the reliability value of pixel in the reliability region is, the greater the probability of this point being a detected point is. The reliability area of the cylinder is represented in the same way, as shown in Fig.7. The higher the reliability of the detected points is, the higher the accuracy of reconstructing the contour of the environment will be.

D. Feature Point Extraction based on Adjacent Pixel Clustering

Reliability regions consist of multiple contact points in Fig.6 and Fig.7 (c). The reliability of the pixel points in each area is between 0 and 1, and there is an extremum, i.e. the optimum solution of detected points. These points are found and used to fit straight segments and discrete arcs, which can reconstruct the environment contour and to improve estimation accuracy.

The specific procedures are as following steps. Pixel points of each reliability region is first clustered. The cluster method is to search every pixel in its 8 fields and put these pixel points with adjacency relationship into one set. In the clustered pixels, the most reliable point is found that are most likely to be contact with the wall for reconstructing the environment contour. The flow chart of the clustering algorithm adopted in this paper is shown in Fig.8. And the steps are summarized as follows: Step 1: To initialize the storage space and establish an empty link list. Each node of the list stores an array and the category tag value is initially set to 1. Step 2: In the reliability regions, to sample a pixel and determine whether the sampling point is classified and identified. If yes, repeating resample procedure. If not, to create a new node in the link list, whose classification value is the current category, and store it in the current node. Then, the current node is inserted into the tail of the list and to go to Step 3. Step 3: To search these pixels

adjacent to the above-mentioned pixel by scanning 8 adjacent fields. If find, the adjacent points are marked as the current category and push it into the stack. Then this step is repeated until the adjacent pixels are not found, go to step 4. Step 4: To determine whether the current stack is empty. If not empty, pop the pixel at the top of the stack and to go to Step 3. If empty, go to step 5. Step 5: The current category tag value is added with one and the algorithm determines whether there are any unmarked points (pixels) in any other reliability areas. If any, return to step 3, if not, end scanning procedure, and go to step 6. Step 6: Find the point with the highest reliability as the detected point in the clustered point set. After processing by using the above-mentioned steps, adjacent pixels in each reliability region are grouped into a class and stored in an array of link list node. What's more, the point with the highest reliability is found as the detected point, which lays a foundation for reconstruction of accurate environment contours in the future.

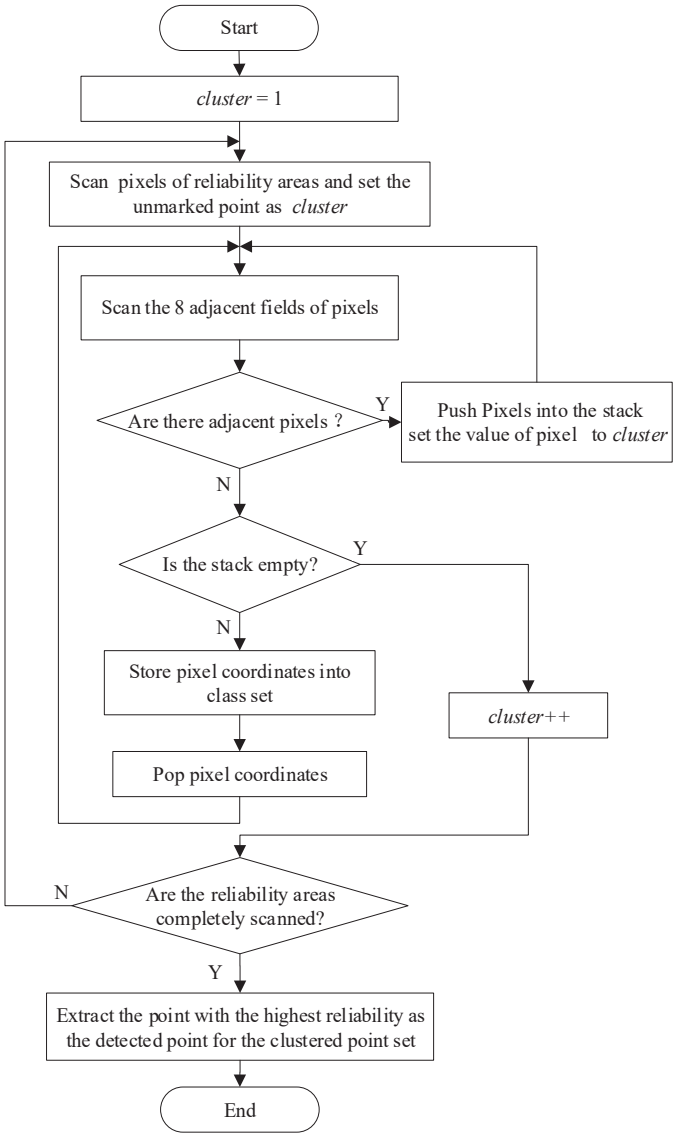

Fig.8 Flow chart of extracting detection point in reliability area based on clustering adjacent pixels.

IV. LEAST SQUARE DETECTION BASED ON EHT

After extracting the detected points (i.e. the feature points) from the reliability areas, we reconstruct the environment contours by using EHT and LSM. Firstly, the feature points are accurately classified using the deviation discriminant in EHT. Then we adopt LSM to perform line and discrete circles fitting on the classified feature points, and the environment contours are finally represented.

A. The Basic Principle of HT

Duda and Hart introduced polar coordinates into HT[26]. This parameterization method has also been widely adopted by later researchers, and its expression is as follows:

$$\rho = x \cdot \cos\theta + y \cdot \sin\theta \tag{9}$$

Where ρ is the perpendicular distance from the origin of the image space to the line to be represented (i.e. vertical distance from origin to line), and θ is the angle between normal line through the origin of the image space and the x-axis. This polar method is equivalent to use a normal vector to represent a straight line, as shown in Fig. 9 (a). In this paper, these parameters are used to represent the straight line of the environment contour.

According to Eq.9, the points in the original image space correspond to the sinusoidal curves in the parameter space, that is, mapping relations have a point-sinusoidal curve duality, as shown in Fig. 9 (b). According to the characteristics of HT, the collinear points in the image space is mapped into the sinusoids in the parameter space, and these sinusoids will intersect at a point. And the accumulated number at the intersection point is the voting value. The higher the voting value is, the higher the probability that the point corresponding to the line will be. As for circle detection, HT can also be similarly used by extending it to Random Hough Transform (RHT).

B. LSM for Fitting Straight Line

RHT method is used to screen the feature data, and then LSM is adopted to fit the screened data and obtain higher accuracy. This procedure is also implemented in the later cylinder identification. LSM is a classical linear regression method, which can obtain the regression line with the smallest mean square error. The basic principle of this method is described as follows.

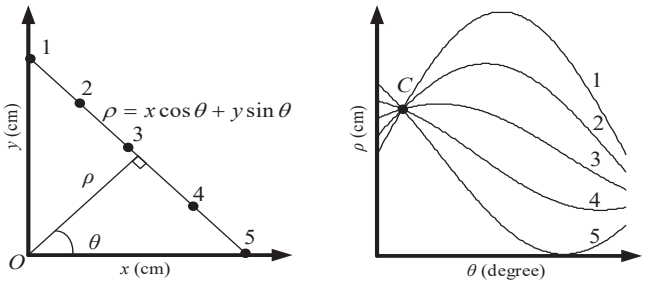

(a) Linear parameterization. (b) Point-sinusoidal duality.
Fig.9 HT principle explanation

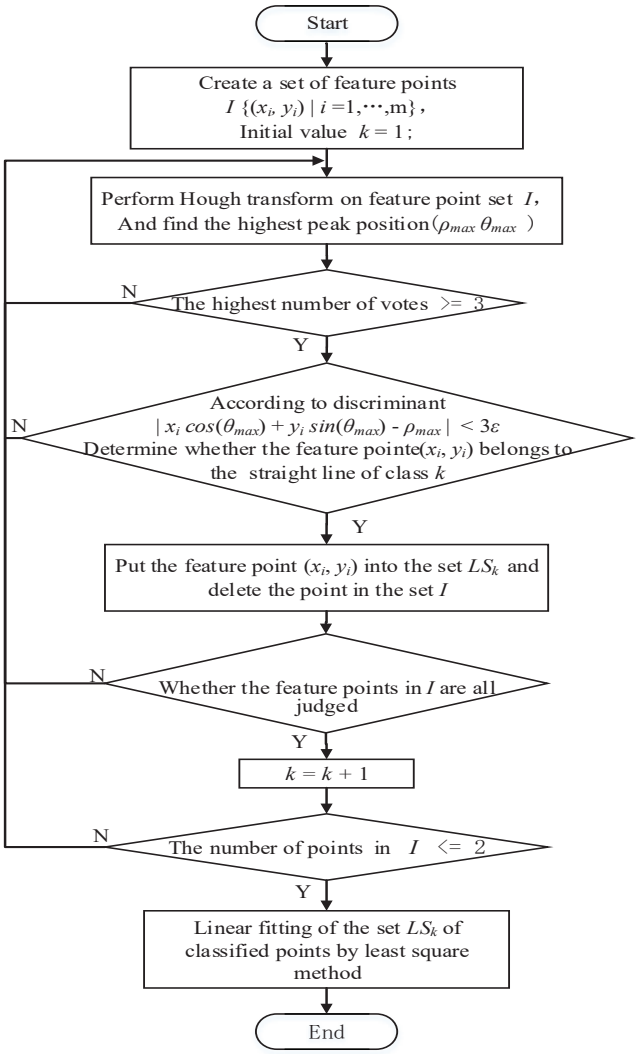

Fig.10 Environmental contour fitting flow chart based on HT and LSM.

Assume that the equation of line to be estimated (i.e. a straight line representing the environment contour) is $y = a \cdot x + b$, including the undetermined coefficients a, b, and the given data set $\{(x_i, y_i)|i = 1, \cdots, n\}$. After substituting these data points into the equation, the error indicator E is:

$$E = \sum_{i=1}^{n} (ax_i + b - y_i)^2 \tag{10}$$

When the error E is the minimum, the partial derivative of the linear parameters a, b is equal to 0 as follows:

$$\begin{cases} \partial E/\partial a = 2\sum(y_i - a_i x_i - b)x_i = 0 \\ \partial E/\partial b = 2\sum(y_i - a_i x_i - b) = 0 \end{cases} \tag{11}$$

Then we get the linear equations about a, b:

$$\begin{cases} (\sum x_i^2)a + (\sum x_i)b = \sum y_i x_i \\ (\sum x_i)a + nb = \sum y_i \end{cases} \tag{12}$$

We set $A = \sum x_i^2, B = \sum x_i, C = \sum y_i x_i, D = \sum y_i$, and the equations are simplified as:

$$\begin{cases} Aa + Bb = C \\ Ba + nb = D \end{cases} \tag{13}$$

To solve a, b, the solution of the equations is:

$$\begin{cases} a = (Cn - BD)/(An - BB) \\ b = (AD - CB)/(An - BB) \end{cases} \tag{14}$$

C. Environmental Straight Line Contour Reconstruction Using EHT and LSM

After obtaining the feature points of the reliability areas, the deviation discriminant based HT called as EHT and LSM are combined for reconstructing environment contour. The specific procedure is shown in Fig.10. This method is that we map the feature points into the parameter space and find the highest peak of voting (the highest point of voting total) to get the corresponding (ρ_{max}, θ_{max}) , as shown in Fig.11, and then the feature points are classified according to the deviation discriminant. The deviation discriminant is defined as

$$| \, x_i \cos(\theta_{max}) + y_i \sin(\theta_{max}) \, | \leq 3\epsilon \tag{15}$$

Where x_i and y_i are the feature point coordinates and ϵ is the distance error of the ultrasonic sensor measurement. When x_i and y_i satisfy this formula (15), the feature points belong to the current category. When all of the points in the feature set are judged or the number of points is less than 2, the judgment procedure is ended. The dots of different colors in Fig 12 are the classified points. Then the classified points are fitted using LSM to reconstruct the environmental contours.

D. Circle Detection Using Random Sampling Consensus based HT

1) Circle detection method based on Random Sampling Consensus based HT: Random Sampling Consensus (RANSAC) [27, 28] based HT also called as EHT is proposed to detect circle. The traditional RANSAC and HT are mainly for some circles with particularly obvious boundaries. However, for some circles with discrete boundaries, they are difficult to be identified by some traditional methods. The algorithm in this paper makes some improvements based on these traditional algorithms, so that it can identify the circle. The algorithm can be roughly divided into three main steps; these steps are detailly represented as follows:

① Detection of circle In detection of the circle, RANSAC and HT are mainly used, and three points are randomly selected from all the discrete pixel points, and a circle is formed based on the three points. Then a ring is formed based on this circle, all the pixels contained in the ring are stored into an array, and the number of pixel points is counted. The circle is divided into several different sector regions according to a certain angle, then the number of pixel points in each annular-sector region is counted and to calculate the variance of the number of pixel points in each region. After that, the circle proportion is defined as statistic quantity, which is the total pixel number dividing the number of the sector region that should contain the pixel points.

② Extraction of the best circle In Step 1, circle corresponding to the total number of pixels is generated, which are sorted according to the circle proportion in a descending order. Take the first ten circles with larger circle proportion. Among the

top ten circles, the circle with the smallest variance is selected as the best circle.

③ Deleting data points of the best circle. Multiple experimental result illustrate that the circle obtained by the above-mentioned method is the one we need. Then the circle is displayed and the pixels around it are marked. These pixels are then removed from the total pixels and then the next circle will be detected similarly. After these three steps are completed, one circle is obtained and loop is repeated again for continuing to find other circles until all the circles are found.

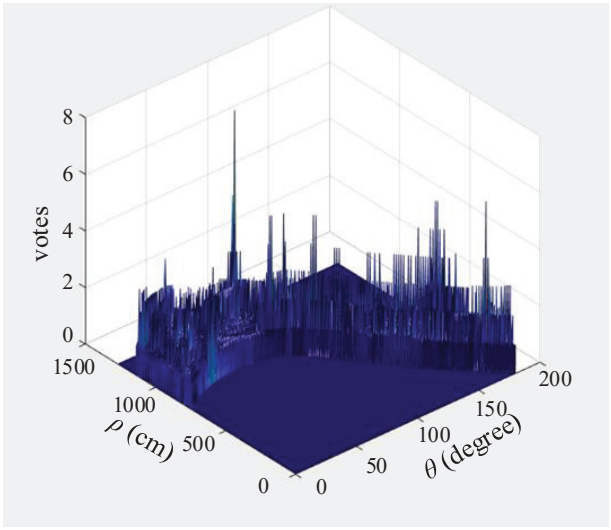

Fig.11 Highest peak extraction of hough transform.

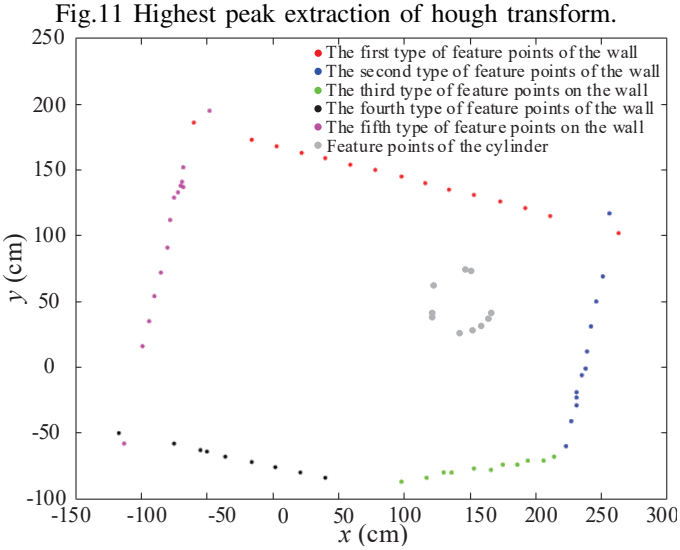

Fig.12 Feature point classification diagram based on hough transform.

2) Circle fitting method using LSM: We suppose a series of data points x_i, y_i near a circle, and fit these points by using LSM to optimize the parameters of the circle [29]. The circular equation is $(x-x_c)^2+(y-y_c)^2=R^2$. The fitting of LSM requires that the sum of the squares of the distances f is the smallest,

$$f=\sum((x_i-x_c)^2+(y_i-y_c)^2-R^2)^2 \tag{16}$$

We define an auxiliary function $g(x,y)$,

$$g(x,y)=(x-x_c)^2+(y-Y_c)^2-R^2 \tag{17}$$

Then the expression (16) can be expressed as:

$$f=\sum g(x_i,y_i)^2 \tag{18}$$

According to the usual steps of LSM, it can be seen that f takes the extreme value corresponding to the following conditions:

$$\begin{cases} \frac{\partial f}{\partial x_c}=0 \\ \frac{\partial f}{\partial y_c}=0 \\ \frac{\partial f}{\partial R}=0 \end{cases} \tag{19}$$

Solve the fitted center coordinate (x_c, y_c) and radius R:

$$x_c=\frac{S_{uuv}S_{uv}-S_{uuu}S_{vv}-S_{uvv}S_{vv}+S_{uv}S_{vvv}}{2(S_{uv}^2-S_{uu}S_{vv})}+x \tag{20}$$

$$y_c=\frac{-S_{uu}S_{uuv}+S_{uuu}S_{uv}+S_{uv}S_{uvv}-S_{uu}S_{vvv}}{2(S_{uv}^2-S_{uu}S_{vv})}+y \tag{21}$$

$$R=sqrt(\sum((x_i-x_c)^2+(y_i-y_c)^2)) \tag{22}$$

Where these items are as follows:

$$\begin{cases} x=\sum x_i/N \quad y=\sum y_i/N \\ S_{uuu}=\sum u_i^3 \quad S_{vvv}=\sum v_i^3 \\ S_{uu}=\sum u_i^2 \quad S_{vv}=\sum v_i^2 \\ S_{uv}=\sum u_i v_i \quad S_{uuv}=\sum u_i^2 v_i \ S_{uvv}=\sum u_i v_i^2 \end{cases} \tag{23}$$

V. UNCERTAINTY ANALYSIS AND PARAMETER SETTING

In the procedure of environmental contour reconstruction using measurement data of the ultrasonic sensor, the noise of the ultrasonic sensor has a great influence on the environmental contour reconstruction. This section calibrates the error distribution of the sensor detection, and the parameter Th setting in the section II, performs experimental testing, and discusses estimation of detection range of the cylinder radius.

A. Estimation of measurement uncertainty of ultrasonic sensor

In this paper, an HC-SR04 ultrasonic sensor is used to detect the distance between the sensor and the wall for calibrating the ultrasonic sensor noise. The measurement scheme is to measure the contour of the wall surface by a group of three positions in the horizontal direction with separation distance l_{step}, as shown in Fig.13(a). Also 12 groups of the positions are designed vertically with the same interval distance l_{step}. First group of positions is 30 cm away from the wall surface, other groups are separated with l_{step} = 20cm. Each group includes 50 times of measure data. As for each measurement, $d=R_{2d}-R_2$, the value d should be 0 in theory. Due to noise disturbance, the error data distribution should theoretically satisfy the Gaussian distribution, and the experimental results are statistically consistent with the Gaussian distribution shown in Fig.13(b), where μ is 0.23cm, σ is 0.32cm, and the statistical result σ is consistent with the error range 0.3 cm given in the ultrasonic sensor manual, and the μ falls within the error range.

B. Parameter Setting and Measurement Testing

Based on the abovementioned uncertainty calibration, σ is used as Th to distinguish between wall and cylinder. The traditional Hough transform (HT) can recognize the contour of linear environment well and the cylindrical contour. However, the calculation is large and the complexity is relatively high. Therefore, the random Hough transform (RHT) is adopted to reduce the calculation amount. The proposed algorithm adopts RHT for pre-processing of the measured data to reduce the noise influence. Fig. 14 represents that cylinder data is obtained when Th is set as σ, and the cylinder with the cylinder radius of 6.77cm, 11.37cm, 15.37cm and 19.90cm can be detected. The detection range of the cylinder radius is related to ultrasonic sensor uncertainty variance σ, the interval distance between the adjacent positions of the ultrasonic sensor, and the distance from the cylinder to the sensor position, which is discussed in the following part.

C. Discussion on Measurement Range of Cylinder radii

Fig.15 shows that three positions abased ultrasonic sensor detection is adopted to measure the cylinder contour. Through deep analysis of the measurement procedure, the conclusion is obtained that detection effect of the cylinder with different radii are related with sonic sensor detection variance σ, the interval distance l_{step} between adjacent positions of sensor detection, and the distance L from the cylinder to the sonic

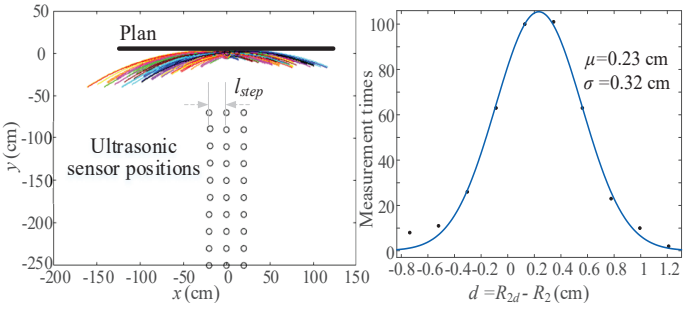

(a)Uncertainty calibration. (b) Fitting of noise distribution

Fig.13 Noise distribution analysis of the sensor range data.

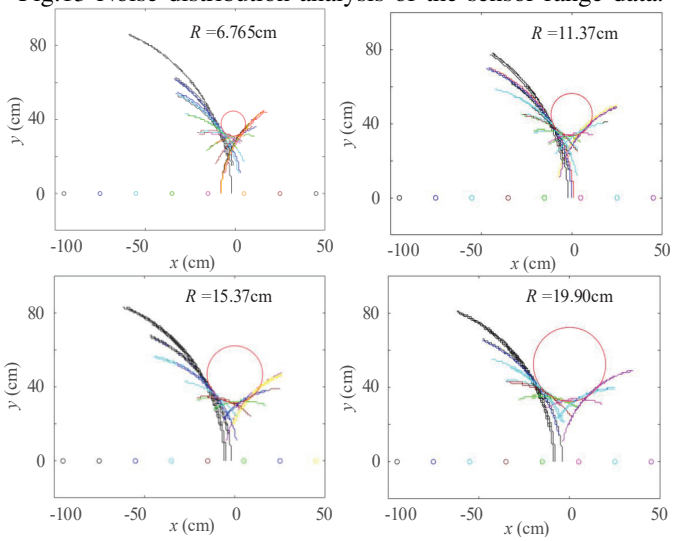

Fig.14 Detection of cylinders with different radii using $Th = \sigma$.

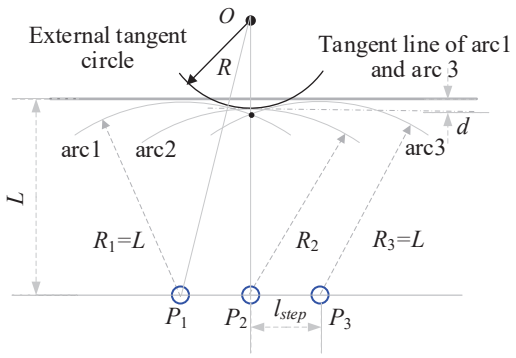

Fig.15 Measurement range of cylinder radii using different d, l_{step} and L.

sensor. In order to simplify the analytical model, this assumes that the ultrasonic sensor detects a cylinder with a radius R directly above three adjacent positions P_1, P_2, P_3, and the spacing distance d for distinguishing the wall and the cylinder is with threshold $Th = \sigma$. And the relationship of the variable is represented using expression (24), where $R_1 = L$, $R_2 = L - d$, R is the radius of the measuring cylinder, which is related to the setting of d. Since d is relatively small, the constant term d in Equation (25) is omitted for approximation. It can be seen that the detection radius R of the cylinder will reduce with d increasing, l_{step} decreases and L increasing. In this experiment, $d = \sigma = 0.32$ cm, $l_{step} = 20$ cm, and the upper bound of the measurement of R is obtained. This value is directly related to the distance L from the ultrasonic sensor to the cylinder. The smaller L is, the larger the upper bound of R is. Fig. 14 show that cylinder contour can be recognized when L is 30 cm. When the cylinder is relatively small, the reflection area of the ultrasonic contacting cylinder becomes smaller, the ultrasonic return rate decreases, and the ranging error increases. Therefore, threshold Th of d is enlarged to 3σ, and $R = 104.16–L$ is obtained. When L is 30 cm, 70 cm, the cylinder can be detected. When L exceeds 104.16 cm, the cylinder measurement data in the test is difficult to be used for distinguishing the wall and the cylinder that is, exceeding the detection range of the cylinder radius, which verifies the rationality of the analysis expression.

$$(R_1 + R)^2 = l_{step}^2 + (R + R_2 - d)^2 \tag{24}$$

$$\begin{aligned} R &= \frac{l_{step}^2}{4d} + d - L \\ &\approx fracl_{step}^2 4d - L, \text{if } l_{step} = 20, d = \sigma = 0.32 \\ &\approx 312.5 - L, \end{aligned} \tag{25}$$

VI. EXPERIMENTAL VERIFICATION AND ANALYSIS

The experimental verification was carried out using an ultrasonic sensor (HC-SR04), a drive motor (28BYJ-48 stepper motor), and a control device (C8051F340 single chip development board), and the devices used in the experiment are shown in Fig.16. Here the ultrasonic sensor is standard module, which provides range information directly. On the foundation of

the above-mentioned theoretical methods, a pentagonal indoor experimental environment was built using a drawing board as show in Fig. 17(a). We planed the measurement positions in the experimental environment. As shown in Fig. 17(b), from the starting point (start), the measurement position was designed along the rectangular path, and the end point (end) meets the start finally. Then, the ultrasonic sensor connected to stepper motor is controlled by a single-chip microcomputer, and the contour of the surrounding environment is measured with an interval of 22.5°in the range of -135°to +135°around the measuring direction of the path. The ultrasonic sensor model and the DSmT fusion method are combined to process multiple measurement results to obtain reliability region including the contact points, as shown in Fig.17(c), and the

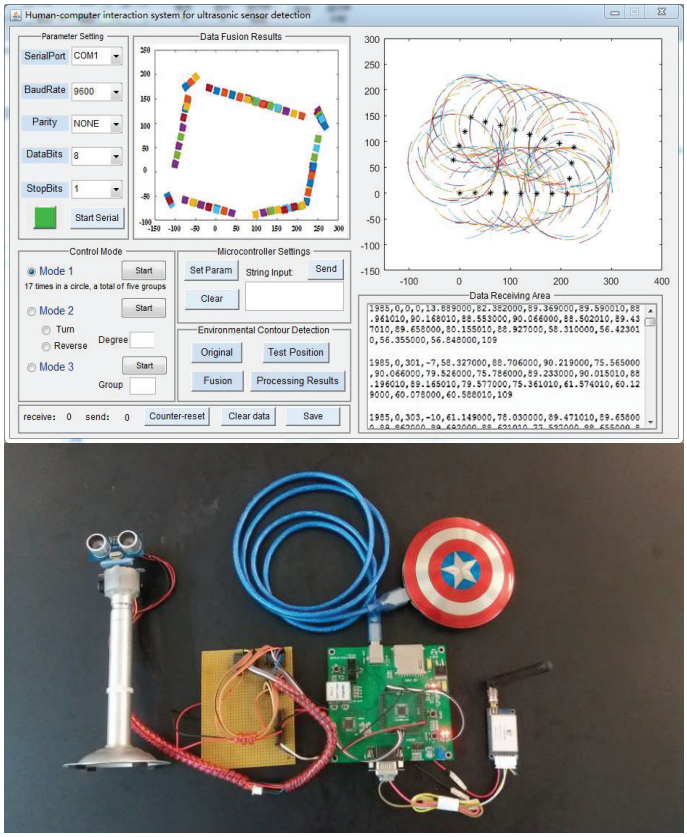

Fig.16 Device for detecting the contour of the environment.

(a) Indoor experimental environment.

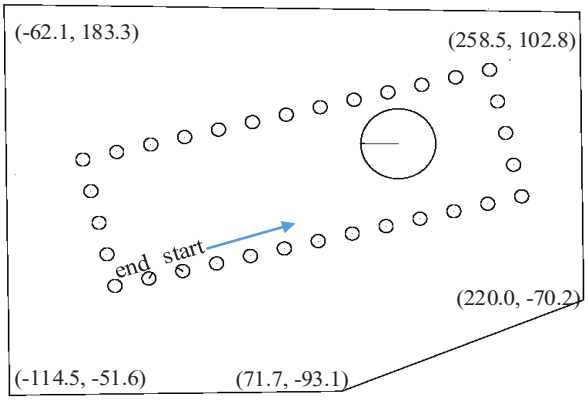

(b) Planned ultrasonic sensor measurement position.

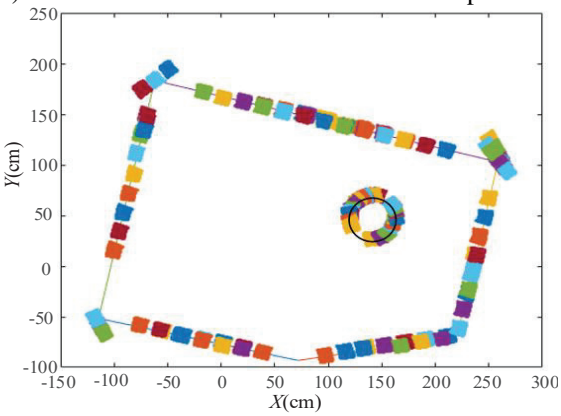

(c) DSmT-based credibility area estimation.

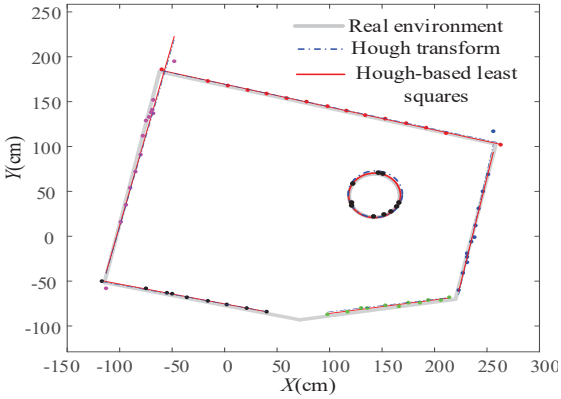

(d) Environment Contour Recognition based EHT and LSM.

Fig.17 Detection results of environmental contours.

feature points are extracted in Fig.17(d). After that, EHT and LSM are combined to fit the feature points into a straight line or a circle, and the environmental contour is estimated, as shown by the thick line in Fig. 17(c). Finally, traditional HT and LSM fitting environment contours are compared with the fitting method proposed in this paper, as shown in Fig. 18, where the line segments labeled 1-5 are the original contours the points A-E represent the intersections of the five line segments, the circle labeled 6 are the cylindrical contours, and F is the position of the cylinder. These several kinds of contours represents the original intersection and position of features, and the estimated environmental contours (including straight and cylindrical parts) for both methods by using three different marks.

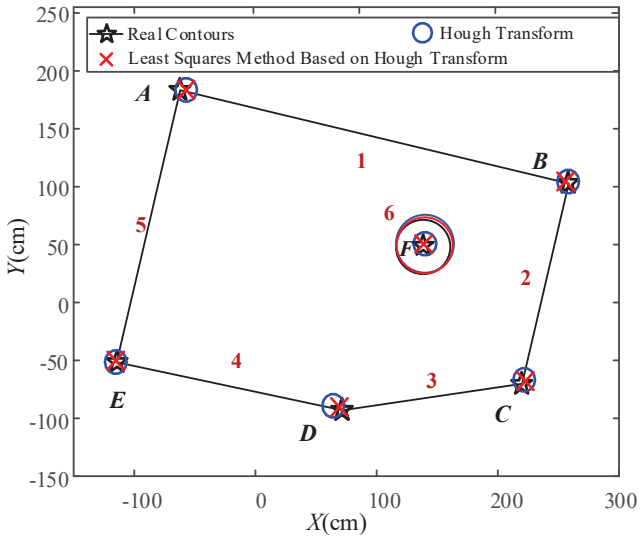

Fig.18 Comparison of intersection points of the real and estimated environment contours.

TABLE I: Comparison of raw and estimated environmental contours data. (cm).

		Real Data	HT	EHT and LSM
1	θ(rad)	1.3248	1.3265	1.3211
	ρ(cm)	162.658	164.3347	164.2017
2	θ(rad)	2.9226	2.9322	2.9474
	ρ(cm)	-229.996	-230.9292	-231.4263
3	θ(rad)	1.724	1.7104	1.7206
	ρ(cm)	-102.9515	-97.3285	-99.952
4	θ(rad)	1.3515	1.3614	1.3536
	ρ(cm)	-75.2727	-73.8178	-73.5764
5	θ(rad)	2.9221	2.8972	2.8997
	ρ(cm)	100.5188	99.5121	99.9550

TABLE II: Comparison and error of coordinates of intersection points of environmental contours line. (cm).

Real Data(cm)			HT		EHT and LSM	
			coordinate (cm)	error (cm)	coordinate (cm)	error (cm)
A	x	-62.1	-56.8	5.305	-57.525	4.65
	y	183.3	183.527		184.127	
B	x	258.5	258.394	2.143	256.335	2.519
	y	102.8	104.941		104.087	
C	x	220	221.823	3.588	222.586	3.749
	y	-70.2	-67.11		-67.486	
D	x	71.7	-67.11	8.079	69.248	3.479
	y	-93.1	-89.202		-90.632	
E	x	-114.5	-115.266	0.994	-115.265	1.859
	y	-51.6	-50.966		-49.906	
	$averageerror$:			4.002		3.251

TABLE III: Comparison and error of environmental contour cylinder parameters (cm)

Real Data(cm)			RHT		EHT and LSM	
			coordinate (cm)	error (cm)	coordinate (cm)	error (cm)
F	x	138.4	139.9	3.17	139.6	1.853
	y	48.0	50.8		49.3	
	R	44.8	47.8	3.0	46.3	1.5

The data in Table 1 is comparison of the real and estimated environmental contours of line data. The data in Table 2 is the contour intersection point coordinates of EHT and LSM, and the intersection point error of the experimental results compared with the real environment. Comparing the average error in the table, the average error of HT is 4.02, and the average error of EHT and LSM is 3.25. It can be seen that the second method has a smaller error. The data in Table 3 is the actual and estimated data of center and radius of the cylinder contour in the experimental environment. It can be seen that the environmental cylinder contour error estimated by EHT is smaller. From the data in Table 2 and Table 3, we can get that the error of the straight line and the cylinder data obtained by EHT and LSM is relatively smaller, and the obtained contours are also more accurate, that is, the estimated contours using the proposed method are closer to the real environment contours, which illustrate the effectiveness of the proposed method.

VII. CONCLUSIONS

Although the ultrasonic sensor is cheap and easy to be used, there are uncertainties in the range and the orientation angle of measurement, which cause serious errors in estimating the environment contour. An ultrasonic distance measurement model based on uncertainty representation is first of all proposed through analyzing the working principle of the ultrasonic sensor. Moreover, the multiple measurements are performed for generating the reliability region based on the contact points, and DSmT method is adopted to fuse the data extracted from these region to reduce uncertainty. Next, the EHT and LSM are combined to reconstruct the environment contour. Then the detection uncertainty is analyzed for setting the parameter Th, detection range of the cylinder radius is estimated.Finally, the proposed algorithm and traditional method are contrasted to illustrate the effectiveness of the proposed method. In this work, concerning the measurement error related to corner detection due to a double bounce of the ultrasonic signals, the corner contour can be compensated according to the two walls information, which need further analysis and correction in the future. method has certain reference value for research of environmental information perception of intelligent robots using ultrasonic sensors.

REFERENCES

[1] Y. Dobrev, P. Gulden, and M. Vossiek, "An Indoor Positioning System Based on Wireless Range and Angle Measurements Assisted by Multi-Modal Sensor Fusion for Service Robot Applications," IEEE Access, vol. 6, pp. 69036-69052, Nov. 2018.

[2] D. Vanderelst, J. Steckel, A. Boen, et al. " Place recognition using batlike sonar," Elife, vol.5, pp.1-23, Aug. 2016.

[3] I. Eliakim, Z. Cohen, G. Kosa, Y. Yovel,"A fully autonomous terrestrial bat-like acoustic robot," PLoS Comput Biol, vol. 14, no. 9, pp.1-13, Sep. 2018.

[4] S. J. Kim, B. K. Kim. "Dynamic Ultrasonic Hybrid Localization System for Indoor Mobile Robots". IEEE Transactions on Industrial Electronics, vol. 60, no. 10, pp. 4562 – 4573, Oct. 2013.

[5] S. M. Dos, P. O. Ribeiro, P. Nunez, et al. "Object Classification in Semi Structured Enviroment Using Forward-Looking Sonar " Sensors, vol. 17, no. 10, pp.2235, 2017.

[6] P. A. Plonski, J. V. Hook, C. Peng, N. Noori, and V. Isler,"Environment Exploration in Sensing Automation for Habitat Monitoring," IEEE Trans. Autom. Sci. vol. 14, no. 1, pp.25-38, Jan. 2018.

[7] A. B. Abdessalem , J. Frédéric, P. Calmon, "Quantifying uncertainty in parameter estimates of ultrasonic inspection system using Bayesian computational framework," Mechanical Systems & Signal Processing, vol. 109, pp. 89-110, Sep. 2018.

[8] M. Khodabandeh, A. Mohammad-Shahri, "Uncertainty evaluation for an ultrasonic data fusion based target differentiation problem using Generalized Aggregated Uncertainty measure," Measurement, vol. 59, no. 59, pp. 139 - 144, Jan. 2015.

[9] H. P. Liu, F. C. Sun, B. Fang, and X.Y. Zhang, "Robotic Room-Level Localization Using Multiple Sets of Sonar Measurements," IEEE Transactions on Instrumentation and Measurement, vol. 66. no.1 pp. 2-13, Jan. 2017.

[10] F.J. Álvarez, R. Kuc, "High resolution adaptive spiking sonar" IEEE Trans. on Ultrasonics, Ferroelectrics and Frequency Control, vol. 56, no. 5, pp. 1024-1033, 2009.

[11] J. Reijniers, and H. Peremans. "Biomimetic Sonar System Performing Spectrum-Based Localization," IEEE Transactions on Robotics, vol. 26, no. 3, pp. 1151-1159, Dec. 2007.

[12] N. I. Giannoccaro, L. Spedicato, L. Aiello. "Kernel PCA and approximate pre-images to extract the closest ultrasonic arc from the scanning of indoor specular environments," Measurement, vol. 58, pp. 46-60, Dec. 2014

[13] Y. C. Lee, J. H. Lim, D. W. Cho, W. K. Chung, "Sonar Map Construction for Autonomous Mobile Robots Using a Data Association Filter," Advanced Robotics, vol. 23, no. 1-2, pp. 185-201, 2009

[14] K. Lee, J. B Song. "Development of sonar morphology-based posterior approach model for occupancy grid mapping, ".Robotica, vol. 35, no. 1, pp. 73-84, Jan.2017.

[15] H. J. Ureña, J. J. García, M. Mazo, D. Hernanz, J. P. Derutin, and J. Serot, "Ultrasonic ranging sensor using simultaneous emissions from different transducers," IEEE Trans. on Ultrasonics, Ferroelectrics and Frequency Control, vol. 51, no. 12, pp. 1660-1670, December 2004.

[16] R. Kuc. "Generating B-Scans of the Environment With a Conventional Sonar," IEEE Sensors Journal, vol. 8, no. 1-2, pp. 151-160, Jan.-Feb. 2008.

[17] I. H. Lee, M. C. Lu, C. C. Hsu, et al. "Map Building of Unknown Environment Based on Fuzzy Sensor Fusion of Ultrasonic Ranging Data," Advances in Autonomous Robotics. Springer Berlin Heidelberg, pp. 446-448, Sep. 2012.

[18] X.-C. Lai, C.-Y. Kong, S. S. Ge, and A. A. Mamun, "Online map building for autonomous mobile robots by fusing laser and sonar data, " in Proc. Int. Conf. Mechatronics Autom., pp. 993–998, Jul. 2006.

[19] X. H. Huang, P. Li, M. Wang, "Evidence Reasoning Machine Based on DSmT for Mobile Robot Mapping in Unknown Dynamic Environment," Dec.2009, pp. 753-758.

[20] X. Y. Han, S. Yuan, X. Yan, P. F. Wang and H. M. Mao, "DSmT based Detection Model of the Ultrasonic Sensor for Estimating Indoor Environment Contour," IEEE WRC SARA 2018, PP:296-301.

[21] J. Steckel, A. Boen, and H. Peremans, "Broadband 3-d sonar system using a sparse array for indoor navigation,," IEEE Transactions on Robotics, vol. 29, no. 1, pp. 161–171, 2013.

[22] A. Ochoa, J. Ureña, Á. Hernández, M. Mazo, J. A. Jiménez, M. C. Pérez. "Ultrasonic multi-transducer system for classification and 3D location of reflectors based on PCA". IEEE Transactions on Instrumentation and Measurement, vol 58, no. 9, pp. 3031-3041, September 2009

[23] J. Steckel and H. Peremans, "Spatial sampling strategy for a 3d sonar sensor supporting batslam," Intelligent Robots and Systems (IROS), 2015.

[24] K. Robin, D. Laurijssen, and J. Steckel. "Low-cost one-bit MEMS microphone arrays for in-air acoustic imaging using FPGA's." SENSORS IEEE, 2017.

[25] W. Hu, W. Li, X. Zhang, and S. Maybank, "Single and multiple object tracking using a multi-feature joint sparse representation," IEEE Trans. Pattern Anal. Mach. Intell., vol. 37, no. 4, pp. 816–833, Apr. 2015.

[26] P. Mukhopadhyay, B. B. Chaudhuri, "A survey of hough Transform," Pattern Recognition, vol. 48, no. 3, pp. 993-1010, Mar.2015.

[27] X. Y. Song, T. Jing, S. Yuan, S. Guo, Y. X. Li, " Scanning Line Based Random Sample Consensus Algorithm for Fast Arc Detection," Dec. 2016, pp. 1117-1122.

[28] R.Raguram, et al., "USAC: A Universal Framework for Random Sample Consensus," Pattern Analysis and Machine Intelligence, IEEE Transactions on, vol. 35. No.8 pp. 2022-2038, Aug. 2013.

[29] Z. Lei, T. Gu, Z. Ji, et al. "An adaptive moving total least squares method for curve fitting," Measurement, vol. 49, no.1, pp. 107-112, Mar. 2014.

Shuai Yuan (M'14) received the B.S. and M.S. degrees from Shenyang Jianzhu University, Shenyang, China, in 2000 and 2003, respectively, and the Ph.D. degree in pattern recognition and intelligent system from the Institute of Automation, Chinese Academy of Sciences, Shenyang, China, in 2012. He is currently an Associate Professor with the Shenyang Jianzhu University. His research interests include intelligent robot control, and image processing.

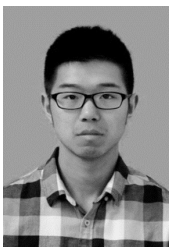

Pengcheng Guo received the B.S. degree in electrical engineering and the automatization specialty from Shenyang Urban Construction College, Shenyang, China, in 2017. He is currently a Master Degree Candidate with the Shenyang Jianzhu University. His research interests in Simultaneous Localization and Mapping.

Xiaoying Han received the B.S. degree from Shenyang Jianzhu University, in 2015. She is currently a student of Dalian University of Technology, majoring in electrical engineering for a master's degree. Her current research interests include wireless energy transfer, energy harvesting, and piezoelectric transducer.

Fangjun Luan received the B.S. degree from Shenyang Jianzhu University, Shenyang, China, and the M.S. and Ph.D. degrees from the University of Jilin, Changchun, China, in 2003 and 2007, respectively. He is currently a Professor with the Shenyang Jianzhu University. His current research interests include pattern recognition and intelligent building. E-mail: luanfangjun@163.com

Feng Zhang received the B.S. degree and M.S. from Shenyang University of Technology, Shenyang, China, in 1998 and the Ph.D. degree from the Institute of Automation, Chinese Academy of Sciences, Shenyang, China, in 2005. She is an associate professor. Her current research interests include mobile robot control, intelligent control.

Tianbo Liu received the B.S. and M.S. degrees from Shenyang Jianzhu University, Shenyang, China, in 1999 and 2006. Professor and Master's Tutor of Shenyang Jianzhu University, His research interests include nanorobotics, intelligent control, and image processing.

Hongming Mao received the B.S degree and M.S degree from Shenyang Jianzhu University, Shenyang, China in 2014 and 2017. Now he is with CCTEG Shenyang Research Institute, and his interests include monitoring hardware and software, and control system design.